J Mater Sci (2007) 42:5223–5228
DOI 10.1007/s10853-006-0604-8

Microstructures and dielectric properties of Y/Zn codoped $BaTiO_3$ ceramics

Bo Li · Shuren Zhang · Xiaohua Zhou · Zhu Chen · Sheng Wang

Received: 25 January 2006 / Accepted: 20 June 2006 / Published online: 23 February 2007
© Springer Science+Business Media, LLC 2007

Abstract The microstructures and dielectric properties of Y/Zn codoped $BaTiO_3$ ceramics sintered in a reducing atmosphere were investigated. XRD analysis indicated the crystal structure of samples change from tetragonal to pseudocubic with increasing Y_2O_3 and ZnO content. SEM micrographs showed Y_2O_3 can suppress grain growth more effectively compared with ZnO, which is ascribed to the presence of second phase $Y_2Ti_2O_7$. Proper amount of Y_2O_3 and ZnO can significantly improve the dielectric temperature characteristics due to the formation of grain core-shell structure. The high performance dielectrics meeting the X7R code were achieved by codoping 1.5 mol% Y_2O_3 and 3.0 mol% ZnO.

Introduction

$BaTiO_3$ with the perovskite structure ABO_3 is generally used as a dielectric material for multilayer ceramic capacitors (MLCCs), which must be modified chemically and physically to produce the required capacitance temperature characteristics [1–4]. The specification X7R requires that the change of capacitance should be less than ±15% over the temperature range from –55 to 125°C. It has been confirmed that the X7R temperature stability is achieved by forming the so-called grain core-shell structure in $BaTiO_3$-based ceramics. The core-shell grain consists of a tetragonal ferroelectric unreacted $BaTiO_3$ core surrounded by a nonferroelectric modified $BaTiO_3$ shell layer [5, 6]. In recent years, X7R MLCCs are widely employed for miniaturization of electronic components because of their temperature-stable dielectric behavior.

$BaTiO_3$–Nb_2O_5–Co_3O_4-based ceramics have been successfully used for fabrication conventional MLCCs with silver and palladium (Ag–Pd) alloy as internal electrodes [5]. In order to reduce the internal electrode cost, nonreducible dielectrics, that can be fired in a reducing atmosphere, by using base metals such as nickel (Ni) and copper (Cu) as internal electrodes have been proposed. Therefore, $BaTiO_3$–R_2O_3–MgO (R represents rare earth elements) based systems have been extensively investigated for their temperature-stable characteristics and nonreducible properties [3, 6].

Both Y_2O_3 [7–9] and ZnO [10] are known as effective additives for improving the microstructures and dielectric properties of single doped $BaTiO_3$ ceramics. However, Y/Zn codoped $BaTiO_3$ materials have not been researched until now. In this study, we develop a new $BaTiO_3$–Y_2O_3–ZnO ternary system for X7R nonreducible dielectrics, and also discuss the microstructures and dielectric properties of Y/Zn codoped $BaTiO_3$ ceramics.

B. Li (✉) · S. Zhang · X. Zhou · Z. Chen · S. Wang
School of Microelectronics and Solid-State Electronics, University of Electronic Science and Technology of China, Chengdu 610054, P.R. China
e-mail: lbuestc@163.com

Experiment procedure

$BaTiO_3$ (Shangdong Guoteng Inc., China) was highly pure hydrothermally synthesized powder with Ba/

Ti = 1.00 and average particle size of 0.4 μm. Reagent grade Y_2O_3 and ZnO were used as dopants and $BaSiO_3$ was used as a sintering aid. The compositions of the specimens were listed in Table 1. The raw materials were mixed by ball milling for 12 h using the deionized water and ZrO_2 balls and then dried and sieved. The obtained powders with an appropriate organic binder were uniaxially pressed into disks with 10 mm diameter and 1 mm thickness. After burning out the binder at 600°C, the disk samples were sintered in a tube furnace at 1,250°C for 3 h in a reducing atmosphere controlled by H_2, N_2, O_2 and H_2O gases. Specimens were annealed at 1,000°C for 1 h in N_2, O_2 and H_2O gas mixture in the cooling stage.

The ceramics were crushed and ground into powder, and then the samples were analyzed by X-ray diffraction (XRD, Philips X' Pert Pro MPD), using Cu Kα_1 X-ray of wavelength 1.54056 Å. The microstructures of the sintered ceramics were observed by scanning electron microscope (SEM, Hitachi S-530). Liquid In–Ga as electrodes was applied on opposite sides of disk samples. Dielectric properties were measured over the temperature range from –55 to 150°C using the capacitance measurement system with an LCR meter (HP4284A) at 1 kHz with 1 Vrms. Insulation resistance was determined by a high-resistance meter in 1 min after applying 100 Vdc at room temperature.

Results and discussion

Figure 1 shows the X-ray diffraction patterns of the samples with different Y_2O_3 and ZnO contents. As indicated in Fig. 1a, both samples YZ1 and YZ2 doped with 0.5 mol% Y_2O_3 show a single tetragonal phase of $BaTiO_3$ solid solution within the XRD resolution limit. The samples containing 1.5 mol% Y_2O_3 show the weak diffraction peaks characteristic of the pyrochlore type $Y_2Ti_2O_7$ (JCPDS 27-0982) phase, confirming that the solubility limit of Y is less than 3.0 mol%. On the other hand, ZnO peaks cannot be detected for all samples in this study. Caballero et al. [10] also reported that ZnO peaks are not observed in the samples with lower amounts of ZnO below 1.0 wt% (about 3.0 mol%), but clearly present in the samples with larger amounts of ZnO above 5.0 wt% in the ZnO-doped $BaTiO_3$ materials. It is thus concluded that the solid solution limit of ZnO in $BaTiO_3$ is about 3.0 mol% in the present system.

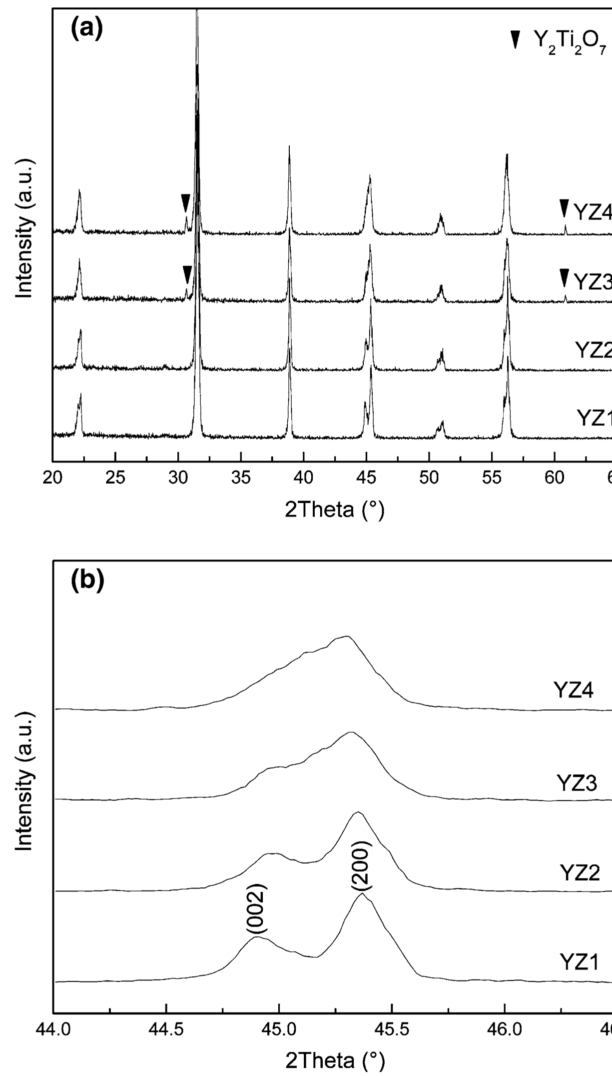

Fig. 1 X-ray diffraction patterns of the samples with different Y_2O_3 and ZnO contents

XRD profiles focusing on the (002) and (200) diffraction peaks are shown in Fig. 1b. The (002) and (200) peaks are separated from each other for sample YZ1, while the distance between two peaks tends to decrease when the amount of Y_2O_3 and ZnO is increased and the two diffraction peaks are merged together almost for sample YZ4. Such remarkable change in the peak profile indicates that the crystal structure of the sintered ceramics change from tetragonal to pseudocubic with increasing Y_2O_3 and ZnO content.

Table 1 Specimen compositions (mol%)

	$BaTiO_3$	$YO_{3/2}$	ZnO	$BaSiO_3$
YZ1	100	1.0	1.0	1.0
YZ2	100	1.0	3.0	1.0
YZ3	100	3.0	1.0	1.0
YZ4	100	3.0	3.0	1.0

The lattice parameters, tetragonality and lattice volume of the samples measured by XRD are presented in Table 2. Both parameters *c* and *a* change for Y_2O_3 and ZnO additions increase, which reveals that the incorporation Y and Zn affect the crystal lattice of $BaTiO_3$. The contraction of the *c*-axis and simultaneous slight extension of the *a*-axis are observed. The tetragonality decreases gradually, which is corresponding with the change of (002) and (200) diffraction peaks. The change of the lattice parameters suggests that this substitution takes place in both A and B sites of the perovskite. According to Shannon's table [11], the ionic radii of Ba, Ti, Y and Zn are summarized as follows: A-site (12 coordinate): Ba^{2+} = 1.610 Å, Y^{3+} = 1.233 Å; and B-site (6 coordinate): Ti^{4+} = 0.605 Å, Y^{3+} = 0.900 Å, Zn^{2+} = 0.750 Å. Y^{3+} and Zn^{2+} substitution in the Ba sites would cause a decrease of the lattice parameters due to the size of Y^{3+} and Zn^{2+} smaller than Ba^{2+}. On the contrary, Y^{3+} and Zn^{2+} substitution in the Ti sites would cause an increase of the lattice parameters due to the size of Y^{3+} and Zn^{2+} larger than Ti^{4+}.

As we know, the ilmenite structure of $ZnTiO_3$ indicates that the Zn cation is too small to support the perovskite structure [12]. Additionally, the ionic radius of Zn is much close to that of Ti ion. Low amount of Zn^{2+} are thus expected to be incorporated in Ti sites and act as acceptors. Since the size of Y^{3+} ion is almost intermediate between those of the Ba^{2+} and Ti^{4+} ions, Y^{3+} ion can occupy either the Ba- or Ti-site in $BaTiO_3$ lattice, depending on the Ba/Ti ratio and its concentration reported by many authors [7, 8]. As mentioned above, the substitution of Zn for Ti site may result in the excess TiO_2. Hence, Y is more favorable to occupy the Ba site and behaves as a donor when the Ba/Ti ratio is less than unity in this study. The recent research showed that the solid solubility limit of Y substitution for Ba site (~1.5 mol%) is much lower than that of Y for Ti site (~12.2 mol%) in the Y_2O_3-doped nonstoichiometric $BaTiO_3$ ceramics [8]. When Y is increased to 3.0 mol%, the extra Y_2O_3 beyond the solubility limit of Ba-site replacement may react with ex-solved TiO_2 to form the $Y_2Ti_2O_7$ second phase, which demonstrates the XRD result shown in Fig. 1a. This result indicates that the solubility limit of Y is lower than 3.0 mol% and that of Zn is about 3.0 mol% in the $BaTiO_3$–Y_2O_3–ZnO ternary system.

Table 2 Lattice parameters, tetragonality and lattice volume of samples

	a (Å)	*c* (Å)	*c*/*a*	*V* (Å^3)
YZ1	3.9948	4.0343	1.0099	64.3811
YZ2	3.9964	4.0278	1.0079	64.3289
YZ3	4.0016	4.0329	1.0078	64.5780
YZ4	4.0037	4.0172	1.0034	64.3942

Figure 2 shows the microstructures development of the specimens doped with various Y_2O_3 and ZnO contents. As shown in Fig. 2 a and b, the specimens containing 0.5 mol% Y_2O_3 exhibit very similar microstructures to each other and abnormal large grains (≥2.0 μm) are observed together with fine grains (≤1.0 μm). However, the proportion of fine grains increases when the amount of ZnO up to 3.0 mol%. This observation is not well compatible with Caballero et al. [10], who reported that ZnO can inhibit grain growth dramatically starting from 0.5 wt% (about 1.5 mol%) in the ZnO-doped $BaTiO_3$ dielectrics. Besides, the small grain is proved not the second phase particles because the corresponding diffraction peaks are not shown in XRD patterns. The samples doped with 1.5 mol% Y_2O_3 show a homogeneous fine-grained microstructure, which coincide with the previous result in the Y_2O_3-doped $BaTiO_3$ ceramics [7]. The average grain size (G_{av}) calculated by linear interception method is about 0.8 μm. Compared with sample YZ3, a further reduction in grain size is observed in the specimen YZ4 with 3.0 mol% ZnO (G_{av} = 0.5 μm). These phenomena thus reveal that Y_2O_3 additives could modify the microstructures more effectively than do the ZnO additives in the $BaTiO_3$–Y_2O_3–ZnO-based system, although both Y and Zn ions act as inhibitors of grain growth in $BaTiO_3$ ceramics. In addition, the $Y_2Ti_2O_7$ second phase identified by the XRD is not detected by SEM due to its minor quantity and well distribution all around the sample. Nevertheless, these intergranularly located second phase particles in samples with 1.0 mol% Y_2O_3 addition have been detected by Lin et al. using TEM microscopic examination [7]. It is considered that a significant reduction in grain size is observed as the Y_2O_3 dopant concentration increased further to 1.5 mol%, which could be explained by the presence of a grain-growth-inhibiting second phase such as $Y_2Ti_2O_7$.

Figure 3 illustrates the temperature dependence of dielectric constant for Y_2O_3 and ZnO codoped $BaTiO_3$ ceramics. Sample YZ1 shows a sharp dielectric peak around Curie temperature (T_C). As ZnO increases up to 3.0 mol%, the dielectric peak intensity of sample YZ2 is depressed dramatically compared with sample YZ1. When Y_2O_3 is increased to 1.5 mol% (especially sample YZ4) the curves become flat over the temperature range from –55 to 150°C. Therefore the increase in Y_2O_3 and ZnO content can significantly improves the temperature dependence of dielectric constant.

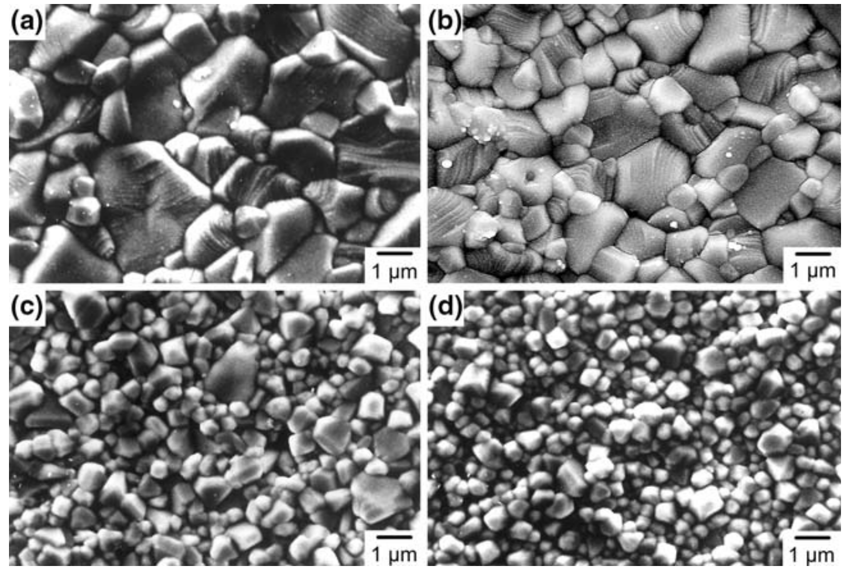

Fig. 2 SEM micrographs of specimens with various Y_2O_3 and ZnO contents (**a**) YZ1, (**b**) YZ2, (**c**) YZ3, (**d**) YZ4

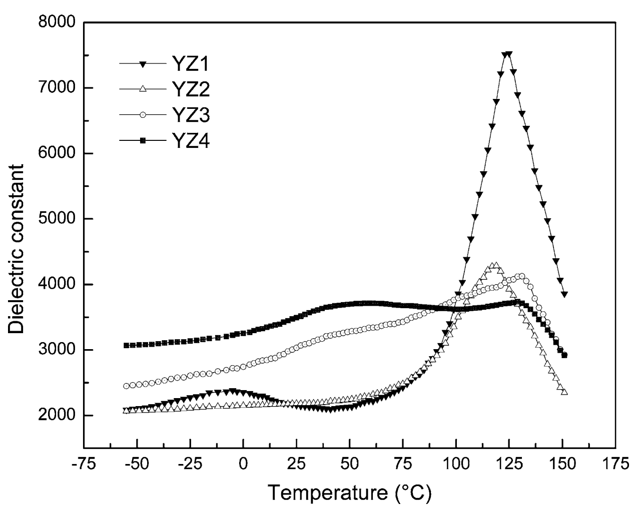

Fig. 3 Temperature dependence of dielectric constant for Y_2O_3/ZnO codoped $BaTiO_3$ ceramics

As shown in Fig. 3, the curves of samples YZ1 and YZ2 exhibit sharp single-peak, while those of samples YZ3 and YZ4 reveal double-peak. This phenomenon is attributed to the formation of grain core-shell structure in the latter two samples. It is considered that Zn could suppress the diffusion of Y into grain core and Zn together with Y reacts with $BaTiO_3$ to form the shell phase. Thus, Zn, like Nb in the $BaTiO_3$–Nb_2O_5–Co_3O_4 [5] and Mg in the $BaTiO_3$–R_2O_3–MgO [6], plays an important role on the core-shell formation in the $BaTiO_3$–Y_2O_3–ZnO system. Furthermore, it was confirmed that the sharp dielectric constant peak at T_C and the broad dielectric constant peak at lower temperature are certainly determined by the volume fraction of grain core and grain shell, respectively [13]. With increasing Y_2O_3 and ZnO content, more dopants diffuse into $BaTiO_3$ grains in depth, leading to the decrease of grain core volume and increase of grain shell. Hence, the sharp dielectric peak at T_C is depressed markedly and becomes broad compared with the former two. For sample YZ4, the dielectric peak intensity at T_C is depressed further, whereas the broad peak intensity as well as the dielectric base intensity at lower temperatures enhance consequently. It can be concluded that both Y_2O_3 and ZnO are helpful to form the core-shell structure, resulting in the increase of dielectric constant at lower temperatures and the flattened temperature characteristic.

The dielectric properties at room temperature (i.e., 25°C) of the samples are shown in Table 3. As illustrated in Table 3, sample YZ1 with 0.5 mol% Y_2O_3 and 1.0 mol% ZnO shows low dielectric constant ($K_{25°C}$) as well as high dielectric loss (tanδ) and small insulation resistivity (IR) at room temperature. However, a drastic decrease in tanδ and increase in IR is observed for sample YZ4 doped with 1.5 mol% Y_2O_3 and 3.0 mol% ZnO. This is predominantly ascribed to the fact that Zn ions occupy the Ti sites and act as acceptor dopants which can effectively prevent the

Table 3 Dielectric properties at room temperature

	$K_{25°C}$	tanδ (%)	IR (Ω·cm)
YZ1	2,154	2.61	10^6
YZ2	2,179	2.02	10^8
YZ3	3,032	1.53	10^{11}
YZ4	3,494	0.69	10^{12}

reduction of $BaTiO_3$ sintered in a reducing atmosphere. Moreover, the high dielectric performance obtained is due to the fine-grained microstructure with relatively high density. These indicate that both Y and Zn can effectively improve the dielectric properties at room temperature.

Furthermore, the sample YZ1 shows two peaks of dielectric constant at about –5°C and 125°C, which is quite similar to the pure $BaTiO_3$ sintered ceramics. The Curie temperature (T_C) is 119°C for sample YZ2 doped with up to 3.0 mol% ZnO and there is 6°C less than T_C of YZ1. For sample YZ3 codoped with 1.5 mol% Y_2O_3 and 1.0 mol% ZnO, T_C increases to 131°C abruptly. Similarly, T_C of sample YZ4 decreases to 129°C for addition of 3.0 mol% ZnO and there is only 2°C lower than T_C of YZ3. This result is consistent with that of Caballero et al. [10], who confirmed that ZnO additions can shift T_C to lower temperature in ZnO-doped $BaTiO_3$ composites. The shift of T_C also reflects the incorporation of Y and Zn cations into the $BaTiO_3$ lattice. Moreover, the addition of ZnO up to 3.0 mol% result in Curie temperature move down, which could be attribute to grain size refinement as well as the formation of oxygen vacancies. Oxygen vacancies are introduced when an acceptor type impurity such as Zn^{2+} replaces Ti site. On the other hand, T_C shifts to higher temperatures as Y_2O_3 increased, which is contrary to the previous results that other large radius rare-earth trivalent ions, such as La and Ce, can effectively shift the T_C of $BaTiO_3$ ceramics to lower temperatures [14, 15]. Moreover, this is in disagreement with Zhi et al., who reported that Y_2O_3 may shift the Curie point to lower temperatures in

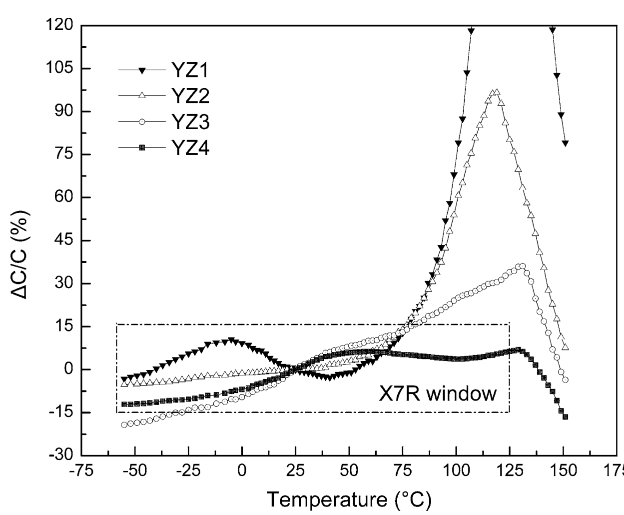

Fig. 4 Temperature dependence of capacitance change ($\Delta C/C$) for Y_2O_3/ZnO codoped $BaTiO_3$ ceramics

$Ba(Ti_{1-x}Y_x)O_3$ ceramics [9]. As previous discussed, the core-shell structure is formed perfectly for both samples YZ3 and YZ4. Sato et al. [16] suggested that a misfit between the grain core and grain shell may give rise to stresses and shift the Curie point to higher temperatures in the $BaTiO_3$–R_2O_3–MgO system, which is quite similar to the current $BaTiO_3$–Y_2O_3–ZnO system.

Figure 4 indicates the temperature dependence of capacitance change ($\Delta C/C$) for Y_2O_3/ZnO codoped $BaTiO_3$ ceramics. Regardless of ZnO content, samples with 0.5 mol% Y_2O_3 show large capacitance variation especially in the high temperature range. With increasing the Y_2O_3 content to 1.5 mol%, the $\Delta C/C$ value at higher temperature drops more abruptly than that at lower temperature. At the same time, further addition of ZnO to 3.0 mol% substantially decreases the $\Delta C/C$ value and results in an improvement of the temperature characteristics. As a result, sufficient amount of Y_2O_3 and ZnO can significantly improve the temperature dependence of the capacitance variation of $BaTiO_3$ ceramics and sample YZ4 codoped with 1.5 mol% Y_2O_3 and 3.0 mol% ZnO is compatible with X7R materials in the present study.

As mentioned above, the grain core is responsible for the $\Delta C/C$ value around T_C, and the grain shell is related to the low temperature $\Delta C/C$ value. The volume fraction ratio of grain core to grain shell determines the $\Delta C/C$–T behavior of the core-shell-structured $BaTiO_3$ ceramics. Accordingly, with increasing Y_2O_3 and ZnO content, the $\Delta C/C$–T behavior of samples is effectively improved which may be ascribed to the decrease of the core/shell volume ratio. Moreover, Armstrong et al. considered that the internal stress resulting from the mismatch between the two regions might be responsible for the improvement of temperature dependence of the dielectric constant [17]. In addition, this flattening effect might be to attributed the existence of the $Y_2Ti_2O_7$ second phase in this system. Although no worse influences of second phase $Y_2Ti_2O_7$ on the dielectric loss and insulation resistance have shown in this study, Sakabe et al. [18] early proposed that the second phase is detrimental to the aspect of the reliability of ceramic capacitors. Thus the exact role of the pyrochlore type second phase for high reliable and stable MLCCs applications should be clarified in the further experiments. Therefore, it is considered that the formation of grain core-shell structure especially the ratio of core to shell is the main reason for improving the temperature characteristics of Y/Zn codoped $BaTiO_3$ materials, while the effect of second phase $Y_2Ti_2O_7$ is only a secondary factor.

Conclusions

The results of XRD confirmed that the solubility limit of Y and Zn is less than 3.0 mol% in the $BaTiO_3$–Y_2O_3–ZnO ternary system. The change of the (002) and (200) diffraction peaks indicated that the crystal structure of the sintered sample changes from tetragonal to pseudocubic with increasing Y_2O_3 and ZnO content. The change of lattice parameters illustrated that Y is favorable to occupy the Ba site and behaves as a donor when the Ba/Ti ratio is less than unity, whereas Zn is expected to be incorporated in Ti site and acts as an acceptor in this study. SEM micrographs showed that Y_2O_3 can suppress grain growth more effectively as compared with ZnO, which is ascribed to the presence of second phase $Y_2Ti_2O_7$. Y_2O_3 additions can shift Curie point to higher temperature while increasing ZnO additives may result in T_C move down. Proper amount of Y_2O_3 and ZnO are helpful to form the core-shell structure and significantly improve the dielectric properties of $BaTiO_3$ ceramics. The formation of grain core-shell structure especially the ratio of core to shell is the main reason for improving the temperature characteristics of Y/Zn codoped $BaTiO_3$ materials, while the effect of second phase $Y_2Ti_2O_7$ is only a secondary factor. The dielectrics containing 1.5 mol% Y_2O_3 and 3.0 mol% ZnO behaved high performance, i.e. $K_{25°C} = 3500$, $\tan\delta = 0.7\%$, $IR = 10^{12}$ Ω·cm, $G_{av} = 0.5$ μm, which satisfy the X7R requirement.

References

1. Kishi H, Mizuno Y, Chazono H (2003) Jpn J Appl Phys 42:1
2. Zhang SR, Wang S, Zhou XH, Li B, Chen Z (2005) J Mater Sci Mater Electron 16:669
3. Wang S, Zhang SR, Zhou XH, Li B, Chen Z (2005) Mater Lett 59:2457
4. Wang S, Zhang SR, Zhou XH, Li B, Chen Z (2006) Mater Lett 60:909
5. Chazono H, Fujimoto M (1995) Jpn J Appl Phys 34:5354
6. Kishi H, Okino Y, Honda M et al (1997) Jpn J Appl Phys 36:5954
7. Lin MH, Lu HY (2002) Mater Sci Eng A 335:101
8. Zhi J, Chen A, Zhi Y, Vilarinho PM, Baptista JL (1999) J Am Ceram Soc 82:1345
9. Zhi J, Chen A, Zhi Y, Vilarinho PM, Baptista JL (1998) J Appl Phys 84:983
10. Caballero AC, Fernández JF, Moure C, Duran P (1997) J Eur Ceram Soc 17:513
11. Shannon RD (1976) Acta Cryst A32:751
12. Dulin FH, Rase DE (1960) J Am Ceram Soc 43:125
13. Park Y, Kim YH, Kim HG (1996) Mat Lett 28:101
14. Kuwabara M, Matsuda H, Kurata N, Matsuyama E (1997) J Am Ceram Soc 80:2590
15. Hennings D, Schreinemacher B, Schreinemacher H (1994) J Eur Ceram Soc 13:81
16. Sato S, Fujikawa Y, Nomura T (2000) Am Ceram Soc Bull 79:155
17. Armstrong TR, Buchanan RC (1990) J Am Ceram Soc 73:1268
18. Sakabe Y, Hamaji Y, Nishiyama T (1992) Ferroelectrics 133:133